Water in Ionic Liquids at Electrified Interfaces: The Anatomy of Electrosorption

Guang Feng,*,† Xikai Jiang,‡ Rui Qiao,*,‡ and Alexei A. Kornyshev*,§

†State Key Laboratory of Coal Combustion, School of Energy and Power Engineering, Huazhong University of Science and Technology (HUST), Wuhan 430074, China, ‡Department of Mechanical Engineering, Virginia Tech, Blacksburg, Virginia 24061, United States, and §Department of Chemistry, Imperial College London, SW7 2AZ London, U.K.

ABSTRACT Complete removal of water from room-temperature ionic liquids is nearly impossible. For the electrochemical applications of ionic liquids, how water is distributed in the electrical double layers when the bulk liquids are not perfectly dry can potentially determine whether key advantages of ionic liquids, such as a wide electrochemical window, can be harnessed in practical systems. In this paper, we study the adsorption of water on electrode surfaces in contact with humid, imidazolium-based ionic liquids using molecular dynamics simulations. The results revealed that water molecules tend to accumulate within sub-nanometer distance from charged electrodes. At low amount of water in the bulk, the distributions of ions and of electrostatic potential in the double layer are affected weakly by the presence of water, but the spatial distribution of water molecules is strongly dependent on both. The preferential positions of water molecules in double layers are determined by the balance of several factors: the tendency to follow the positions of the maximal absolute value of the electrical field, the association with their ionic surroundings, and the propensity to settle at positions where more free space is available. The balance between these factors changes with charging the electrode, but the adsorption of water generally increases with voltage. The ion specificity of water electrosorption is manifested in the stronger presence of water near positive electrodes (where anions are the counterions) than near negative electrodes (where cations are counterions). These predictions await experimental verification.

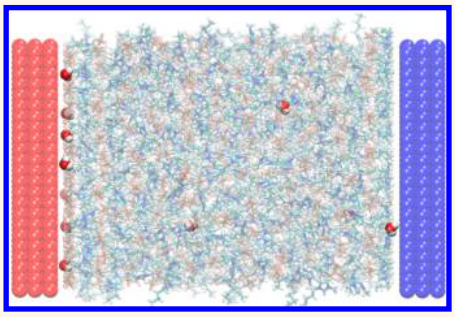

KEYWORDS: water electrosorption · ionic liquids · electrical double layer · water–ion association · molecular dynamics

Room-temperature ionic liquids (RTILs) are an emerging class of ionic materials that are made entirely of ions but have melting points close to room temperature.[1−3] RTILs have many useful properties[4−6] such as low volatility, high thermal stability, and wide electrochemical windows. These properties, along with the fact that the physicochemical properties of RTILs can be manipulated by tuning the functionalization and/or combination of their ions, make RTILs potentially ideal materials for electrochemical applications such as energy storage, electrode kinetics, electrodeposition, and nanotribology.[7−14] For example, when used as electrolytes, RTILs' wide electrochemical window enables supercapacitors to operate at voltages much higher than those afforded by conventional electrolytes, thereby greatly increasing their energy density and thus addressing their key limitations.[15−17] Indeed, using RTILs, impressive improvement of supercapacitor performance has already been demonstrated in laboratory systems.[17−22]

Transforming the success of RTILs in well-controlled laboratory systems to more practical systems, however, often must address additional issues. One such issue is the contamination by water. Most RTILs are hygroscopic, and even those featuring hydrophobic ions can absorb a large amount of water from the atmosphere.[23] Because of this, extensive studies have been devoted to the investigation of water–RTIL mixtures, especially for imidazolium-based RTILs.[24−33] It has been discovered that, for up to a dissolved water concentration of ∼0.2–1.0 M in bulk RTILs featuring $Bmim^+$ cations, water molecules mostly exist in the form of monomers (also termed "free" or "solitary" water)[32,34,35] and are often trapped near the hydrophilic moieties of RTILs. While water

* Address correspondence to a.kornyshev@imperial.ac.uk, ruiqiao@vt.edu, gfeng@hust.edu.cn.

Received for review September 5, 2014 and accepted October 23, 2014.

Published online 10.1021/nn505017c

molecules do interact with the aromatic protons of the cation, they interact with anions more strongly[36,37] and often form hydrogen bonds with two anions simultaneously.[32,34] Water can modify both the structure and dynamics of RTILs; for example, high water content in RTILs can lead to a disruption of polar networks,[27,29] strengthening of tail−tail correlations,[27] accelerated self-diffusion of ions,[32,38] and reduced viscosity.[39] Systematic studies have revealed that the extent of the modification of RTILs' structure and dynamics by water depends most strongly on the water content, the nature of anion, and the length of the alkyl chain.[27,32,34,40,41]

While extensive studies of the water−RTIL mixture provided insights into how water affects the properties of bulk RTILs, many issues remain open. In particular, the adsorption of water on electrified interfaces in RTILs has not been investigated. Since completely removing water from RTILs is nearly impossible,[42] it is safe to assume that RTILs in practical electrochemical systems will have at least a small amount of sorbed water. While prior work already suggested that this will not significantly affect the physicochemical properties of water-stable, *bulk* RTILs, what occurs at electrified interfaces can be very different. Specifically, if water molecules exhibit strong preference to become adsorbed on the electrode or in the first ion layer of the electrical double layer (EDL) upon polarizing the electrode, significant accumulation of interfacial water is possible even when the concentration of water in bulk RTILs is low. A high local concentration of water at or adjacent to the electrode surfaces can *potentially* compromise RTILs' key advantages: the electrolysis of the adsorbed water molecules can effectively reduce RTILs' electrochemical window, disturb the target performance, and contribute to degradation of the electrode or, in the case of supercapacitors, to leakage currents.

In this work, we study electrically mediated adsorption of water from bulk humid RTILs onto planar electrodes using molecular dynamics (MD) simulations. We show that, upon electrification, the adsorption of water on electrodes can be greatly enhanced and the degree of enhancement depends on the magnitude/sign of electrode polarization and the nature of ions. The molecular mechanisms of these observations are clarified, and the implications of the enhanced adsorption are discussed.

RESULTS AND DISCUSSION

Figure 1a shows the MD system used to investigate the electrosorption of water on electrified interfaces in humid RTILs. Each system consists of a RTIL/water mixture enclosed between two planar electrodes with opposite surface charge densities (σ = 0, $\pm$0.04,... $\pm$0.20 C/m^2 were examined in a series of simulations; see Methods). Each system is closed and

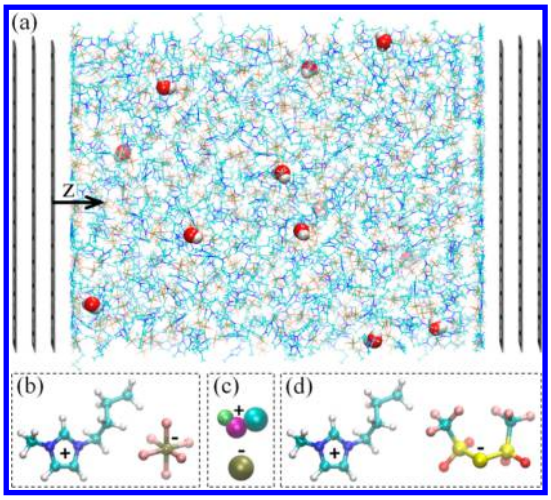

Figure 1. Models of humid ionic liquids between two planar electrodes. (a) Snapshot of the MD system (gray spheres, electrode atoms; color lines, [Bmim][PF$_6$] molecules; red/white spheres, water molecules); (b) all-atom model of the ionic liquid [Bmim][PF$_6$]; (c) coarse-grained model of the ionic liquid [Bmim][PF$_6$]; (d) all-atom model of the ionic liquid [Bmim][Tf$_2$N].

contains 656 pairs of ions and 12 water molecules, the amount consistent with the expectation that water contamination in the bulk of RTILs with hydrophobic ions should not be significant. Both all-atom and coarse-grained models have been used for RTILs to assess the sensitivity of the simulation results with respect to molecular models. Two popular RTILs, [Bmim][PF$_6$] and [Bmim][Tf$_2$N] (Figure 1b−d), were used to assess whether features of water electrosorption observed in our simulations are generic to hydrophobic RTILs, in which ions are larger than water molecules.

Electrosorption of Water and Its Electrochemical Fingerprints. We quantify the adsorption of water on the electrode surface by computing the average number density of water in the region within 0.35 nm from the innermost layer on the electrode, $\overline{\rho}_n^{ad}$. This region is hereafter termed "the interfacial region", and water in it can be considered as contact-adsorbed on the electrode surface given that the van der Waals radii of the electrode atom and the water molecule are ~0.18 and ~0.17 nm, respectively. Figure 2a shows that the adsorption of water on the electrode surface in contact with humid [Bmim][PF$_6$] is, generally, enhanced as the surface charge density of the electrode increases, especially if the electrode is already moderately charged. Since the total number of water molecules in our closed system is the same for each surface charge density considered, we further compute the relative enrichment/depletion of water molecules in the interfacial region compared to those in bulk RTILs. This is characterized by the ratio of $\overline{\rho}_n^{ad}$ to the number density of water in the central portion of the system (between z = 3.5 and 4.5 nm in Figure 1), $\overline{\rho}_n^{bulk}$, where the RTILs are bulk-like. Figure 2b shows that, near neutral or weakly charged negative

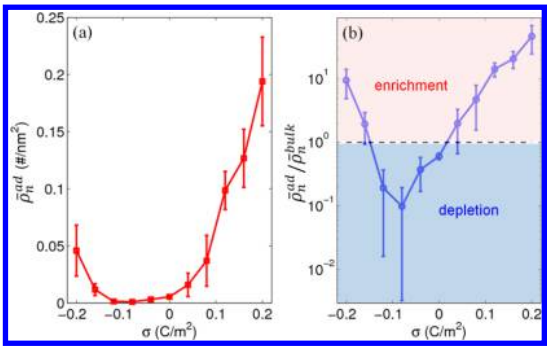

Figure 2. Electrosorption of water on planar electrodes. Evolution of the average number density of water molecules in the interfacial region (a) and the relative enrichment (or depletion) of water molecules in this region compared to that in bulk RTILs (b) as a function of the surface charge density. The interfacial region is taken as 0.35 nm within the innermost layer of the electrode. The RTIL, [Bmim][PF_6], is modeled using the all-atom force fields.

electrodes, there is a water depletion as compared to the bulk, likely due to the hydrophobic nature of the graphite electrode[43] (had we taken into account image forces, the depletion would have been even stronger due to stronger electrostatic attraction of ionic charges than water dipoles to the conducting walls). However, further increase of electrode charge enriches the EDLs with water, and this starts to be seen already near moderately charged electrodes. Additional simulations in which there are more water molecules inside the system showed that such an enhancement is rather insensitive to the humidity of RTILs, at least at low humidities (see Supporting Information Figure S1). For the same magnitude of surface charge density, water enrichment is stronger near positive electrodes than near negative electrodes. We found that the enrichment of water in the interfacial region, following the increase of the surface charge density of the electrode, is also seen for the tested coarse-grained model of [Bmim][PF_6] or if we use a different RTIL, [Bmim][Tf_2N], described by an all-atom model (Figure S2).

The details of the distribution of water in the water-rich domain of the EDL depend on the RTIL model or the type of RTILs. Indeed, already from the considered examples one can see that the positive and negative branches of the enrichment *versus* surface charge density curve are more symmetric for water in [Bmim][Tf_2N] than in [Bmim][PF_6] (see Figure S2). However, the fact that electrification-induced enhancement of water adsorption on electrode surfaces is observed in simulations with different RTILs or their different models suggests that such a phenomenon is generic, at least for the class of RTILs considered here.

To better delineate the electrosorption of water from humidified RTILs, we analyze the detailed structure of the EDLs: the distributions of ions and water molecules near the interface and their mutual effects on each other. All the distributions that we show below are averaged along the plane parallel to the electrode surface. Figure 3a–c shows the number density profiles of water, $Bmim^+$ cations, and PF_6^- anions near electrodes with σ = 0 and ±0.16 C/m^2 (for water at other surface charge densities, see Figure S3a,b). Similar to prior studies,[44–48] the distribution of RTILs near the electrode surface is heterogeneous: cations and anions form alternating layers, and the oscillations of ion density (Figure 3a–c) and nonzero space charge density (Figure 3d–f) extend from the electrode surface up to about 1.5 nm. The structure of interfacial RTILs varies in response to the electrification of the electrode. For example, as σ changes from 0 to −0.16 C/m^2, the first cation layer evolves into two peaks: $Bmim^+$ ions in the first peak are mostly parallel to the surface, while those in the second peak tend to be vertical to the surface (Figure S4).

Near neutral electrodes, the water density profile exhibits a weak peak at z = 0.33 nm and oscillates as it moves toward the bulk (Figure 3b). Water molecules near the electrode exist in the form of monomers due to the low concentration of water "impurities" in our systems (note that, for clarity, the water density profile has been blown up by a factor of 50 in Figure 3b). The water peaks simply indicate that water molecules prefer to accumulate at these positions. Near electrodes with surface charge densities of ±0.16 C/m^2, the peak of the first water density profile shifts to $z \approx$ 0.30 nm and its magnitude increases greatly, especially near the positive electrodes. Water molecules in the interfacial region exhibit distinct orientational ordering: they are oriented quite randomly near neutral electrodes but become strongly aligned with the electrical fields of polarized electrodes (see Figure S3c,d).

For the relatively dry RTIL considered here (water-to-RTIL ratio is ~1:55), water seems to have a limited impact on the distributions of RTILs near the electrode. However, even a minute amount of adsorbed water molecules may alter the electrical properties of the EDL noticeably because a small change of local ion density can notably change the electrical potential inside the EDL. To test this hypothesis, we removed all water molecules from the simulation system and repeated the simulations. We found that the potential drop across the EDL adjacent to the positive electrode of 0.16 C/m^2 increases by ~8% when the water molecules are removed (see Figure S5a). Since the potential drop across the EDL directly controls the capacitance of the EDL, this result indicates that *it may be possible to detect the adsorption of water on the electrode surface through measurement of the differential capacitance*. Further simulations indicated that the differential capacitance at 2 V decreases by ~10% when all the water molecules in the humid [Bmim][PF_6] considered here were removed (see Figure S5b).

Origins of Water Electrosorption. The nonuniform water density profile shown in Figure 3 suggests that the

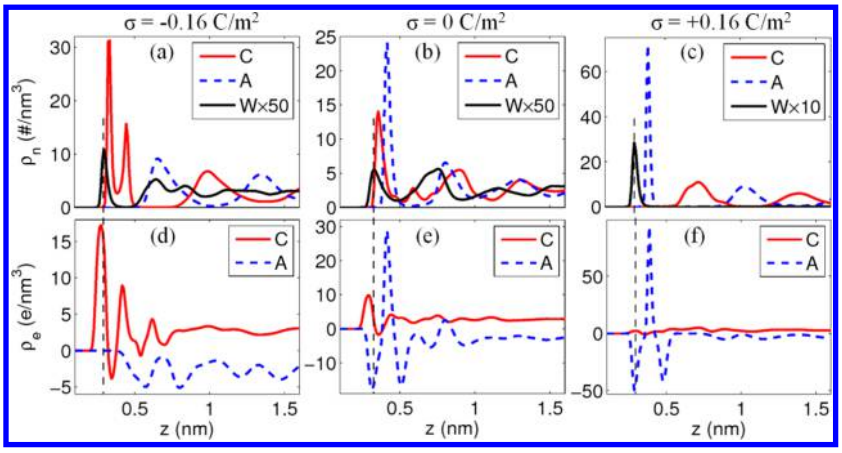

Figure 3. Structure of double layers in humid ionic liquids [Bmim][PF_6]. (a−c) Water and ion number density profiles; (d−f) space charge density contributed by cations and anions. The three columns correspond to electrodes with surface charge densities of 0 and ±0.16 C/m^2. In legends, C is cation; A is anion; W is water (×10 and ×50 means that water density is multiplied by a factor of 10 and 50, respectively). The vertical dashed lines denote the position of the first water peak. The position of water/anion (cation) is based on its geometric (ring) center.

distribution of water molecules near the electrode is intimately related to the structure of the EDLs that would have been formed by RTILs without water. Below, we will focus on how these EDLs and their response to the electrode polarization determine the distribution of water molecules near the electrode surface.

The nonuniform distribution of water molecules near the electrode surface is affected by the distribution of the electrical field inside the EDLs. Because of the overscreening phenomenon, the electrical potential inside the EDLs oscillates over molecular distances as it moves away from the electrode surface, which in turn leads to oscillation of the electrical field (Figure 4a−c). Since water molecules are dipoles, they experience a net force when placed inside an inhomogeneous electrical field. Neglecting the finite size of the water dipole and assuming that it is oriented in the direction of the average electrical field in the EDL, the force experienced by the water molecule is given by $f_z = p(dE_z/dz)$, where E_z is the electrical field in the direction normal to the electrode surface and p is the water molecule's dipole moment. Therefore, a water molecule will move toward the direction with increased $|E_z|$ and tends to accumulate at positions satisfying $dE_z/dz = 0$ and $d^2E_z/dz^2 < 0$ when $E_z > 0$ (or $d^2E_z/dz^2 > 0$ when $E_z < 0$), that is, where the electrical field is at its local maximum (if $E_z > 0$) or minimum (if $E_z < 0$). The position with the largest absolute value of the electrical field in the entire EDL would have been the stable position of water molecules, had they been just point dipoles; correspondingly, the locations where the absolute value of the electrical field reaches local maxima are the metastable positions. Let us, conventionally, call these positions *electrically stable* and *electrically metastable*, respectively.

We computed E_z using the ionic space charge density obtained from MD simulations. Figure 4a−c shows that there exist multiple electrically stable/metastable positions for water molecules near the electrode surface. This, along with the fact that the average electrical field in the bulk of RTILs is zero, helps explaining the preferential accumulation of water at positions near highly charged electrodes rather than in bulk RTILs. As shown in Figure 4a−c, for all electrode charge densities considered here, the peaks of the water density profiles correspond approximately to the electrically stable and metastable positions, though the correspondence is not exact.

The exact correspondence between water peaks and the stable/metastable positions should, in fact, not be expected as water molecules are not "point dipoles"; they have finite volume. The propensity for water molecules to accumulate at the electrically stable and metastable positions defined by the local maxima of the absolute value of electrical field in water-free RTILs (which are hardly shifted by the presence of water), however, cannot fully explain the water distribution shown in Figure 4a−c. For example, near an electrode surface with $\sigma = -0.16$ C/m^2, one expects the water density to be highest at the electrically stable position ($z = 0.45$ nm), but the highest water density peak appears at $z = 0.30$ nm (Figure 4a).

On the other hand, we observe that the water density peaks are correlated with the peaks of the ionic charge density profiles (see Figure 3d−f). Such a distinct correlation originates from the strong local electrostatic interactions between water molecules and their surrounding ionic shells, which causes strong water−ion association. Since water molecules associate much more strongly with PF_6^- ions than with $Bmim^+$ ions,[34,37] the accumulation of water is more significant near the positive electrodes (where the density of PF_6^- ions is high) than near the negative electrodes (where the density of $Bmim^+$ ions is high).

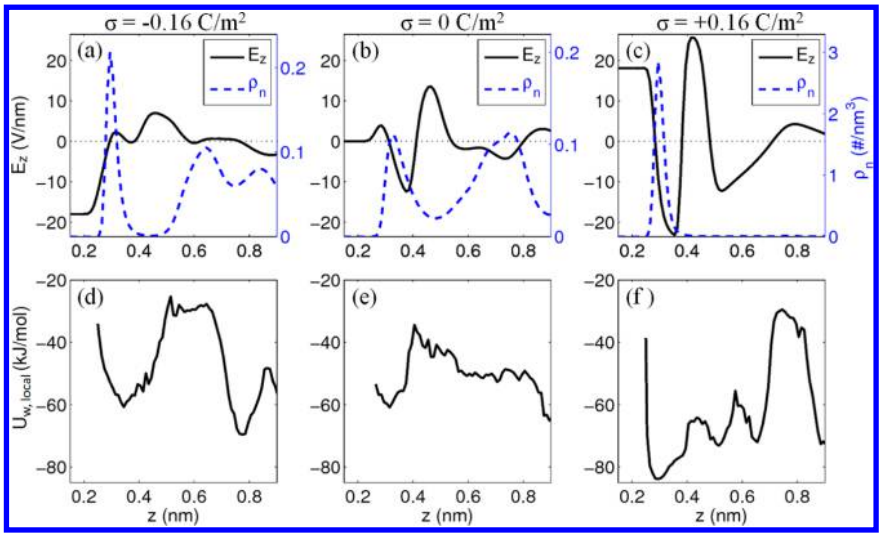

Figure 4. Correlation between the distributions of water density, electrical field, and the "local" potential energy of water molecules in EDLs. Electrical field (a−c, left *y*-axis), water number density (a−c, right *y*-axis), "local" potential energy of water molecules (d−f) are shown as a function of their distance from the electrode surface. The surface charge density of the electrode is (a,d) −0.16 C/m^2, (b,e) 0 C/m^2, and (c,f) +0.16 C/m^2. The "local" potential energy of a water molecule is the summation of the interaction energy of the water molecule with species within 1.1 nm from its oxygen atom, and it signifies the association of a water molecule with its ionic surroundings.

To quantitatively assess the role of ion−water interactions in determining the distribution of water molecules near electrodes, we have evaluated the potential energy of a water molecule at different positions from the electrode surface due to its interactions with nearby species, $U_{w,local}(z)$. Such a potential energy bears similarity with the Madelung potential[49] and its variants,[50] which have been used to characterize the local (non-mean-field) interactions between an ion and its surroundings in an EDL. Specifically, we computed the interaction energy of a water molecule with all species within 1.1 nm from its oxygen atom using a cutoff method (using a different cutoff radius does not qualitatively affect the results). Figure 4d−f shows that $U_{w,local}(z)$ oscillates as it moves from the electrode surface toward the bulk liquids. The peaks of the water density profile correspond quite well to those determined *jointly* by the electrically stable/metastable positions of water dipoles and the minimum of $U_{w,local}$. Specifically, near electrodes with σ = −0.16 C/m^2, while water accumulation is favored at two metastable positions ($z \approx 0.32$ and 0.46 nm), the water density peak appears only at $z \approx 0.30$ nm because $U_{w,local}$ of a water molecule at $z \approx 0.46$ nm is much less negative than that at $z \approx 0.32$ nm (Figure 4d). Similar scenario helps explain why, near electrodes with σ = +0.16 C/m^2, water molecules accumulate mostly at $z \approx 0.30$ nm since the minimum of $U_{w,local}(z)$ is located at $z \approx 0.29$ nm (Figure 4f).

The preferential accumulation of water near neutral electrode surfaces is more complicated (Figure 4e): the combination of the electrical field and $U_{w,local}$ could explain why the first water peak occurs at 0.32 nm; however, it is not clear why there is also a relatively large water peak at $z \approx 0.75$ nm despite the fact that, at this position, the absolute magnitude of the electrical field is quite small and $U_{w,local}$ of water molecules is not very negative.

Thus far we focused on the energetics of water molecules at different positions across the EDL. The results in Figures 3 and 4 suggest that the energetic effects dominate the distribution of water near moderately charged electrodes. The entropic effects play a less important role compared to the energetic effects in the RTILs examined here,[51] but these effects will become more important when the size of ions becomes smaller or comparable to that of the water molecules. Such a situation has not been studied here because most ions in RTILs are larger than the water molecules. The energetics of water molecules, especially the interactions between water molecules and their surrounding ions, are closely related to how ions are distributed around each water molecule. Elucidating such structural details, which depend strongly on the ions' geometrical and chemical characteristics, helps us understand the energetics of ion−water interactions and how the distribution of water inside EDLs is affected by the nature of RTILs. Below, we focus on the distribution of the aromatic protons (hereafter denoted as aH) of the $Bmim^+$ ion and the F atoms of the PF_6^- ions around the water molecules since these highly charged moieties of ions interact most strongly with the water molecules. Figure 5a shows the radial distribution function (RDF) of aH and F atoms around the oxygen atom of a water molecule in bulk RTILs. The large first peak of both RDFs indicates that a water molecule in bulk RTILs exists in a microenvironment that is rich in highly polar moieties,

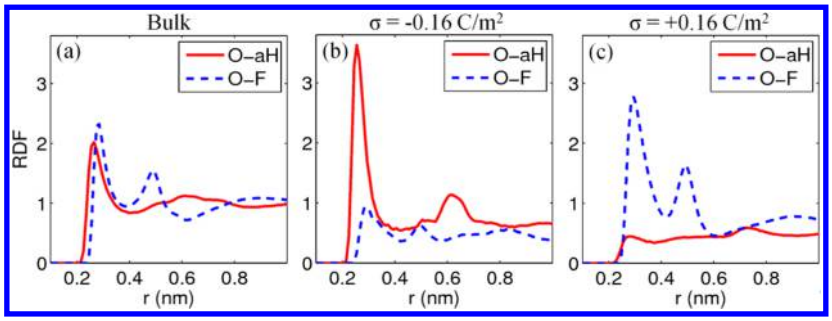

Figure 5. Association of water molecules with highly charged moieties of ions. The radial distribution functions (RDFs) of the cations' aromatic protons (red lines) and the anion's fluorine atoms (blue dashed lines) with respect to the water molecules' oxygen atom in bulk [Bmim][PF_6] (a) and near electrodes with surface charge densities of -0.16 C/m^2 (b) and $+0.16$ C/m^2 (c). The RDFs are obtained by dividing aH and F atom densities at distance *r* from the oxygen atom by the densities of aH and F atoms in bulk RTILs. For oxygen atoms near the electrode surface, their RDFs do not approach 1.0 at large radial distance due to the geometrical confinement by the electrode surface.[52]

which helps explaining the hygroscopic nature of hydrophobic RTILs.

The water molecules near electrodes with $\sigma = -0.16$ C/m^2 exist in a quite different microenvironment compared to that in bulk RTILs: each water molecule within the first interfacial water layer ($z < 0.35$ nm) is surrounded by more aH atoms but less F atoms (Figure 5b). The enhanced access of water molecules to the highly polar aH atoms likely has two origins. First, near negative electrodes, the density of cations is higher than that in bulk RTILs. Second, electrode polarization induces a separation of cations and anions in the interfacial region. Consequently, the water molecules in this region have better access to the cations' highly polar moieties that tend to be blocked by anions in bulk liquids. Specifically, in bulk liquids, PF_6^- ions occupy most of the space near the aromatic protons of a $Bmim^+$ ion because they can form hydrogen bonds with them (each $Bmim^+$ ion forms 1.46 ± 0.04 hydrogen bonds with its surrounding PF_6^- ions). However, near an electrode with $\sigma = -0.16$ C/m^2, each $Bmim^+$ ion is surrounded by fewer PF_6^- ions and the number of hydrogen bonds it formed with these PF_6^- ions also decreases to 0.66 ± 0.04. Therefore, water molecules near the electrode surface have better access to $Bmim^+$ ions' highly charged moieties (*e.g.*, the aH atoms).

The above trend is reversed when the electrode is polarized positively (Figure 5c). These results show that varying the electrode charge (or equivalently, electrode potential) can greatly affect the microenvironment for water molecules near electrode surfaces, thus explaining why the energetics and adsorption of water near electrode surface can be varied greatly by manipulation of electrode charge (see Figures 3 and 4).

Asymmetry of Water Electrosorption. Figure 2b shows that the water adsorption on positive electrodes is generally stronger than on negative electrodes with the same magnitude of charge. As explained above, such an asymmetry is due in part to the stronger interaction of water molecules with the studied anions than with cations. Another factor that contributes to the asymmetry is the different free spaces available to water molecules near positive and negative electrodes. Near positive electrodes, the rather spherical PF_6^- ions approach the electrode surface to a distance of ~0.39 nm (Figure 3c). Since water molecules can approach the electrode surface to a distance of ~0.35 nm, there is some free space between the contact adsorbed PF_6^- ions and the electrode surface where water molecules can settle. Near negative electrodes, the rings of $Bmim^+$ ions approach the electrode surface to a distance of ~0.33 nm (Figure 3a), and they are almost parallel to the electrode surface (Figure S4). Therefore, there is less free space between the electrode surface and contact adsorbed $Bmim^+$ ions for water molecules to accumulate.

CONCLUSIONS AND OUTLOOK

In summary, using molecular dynamics simulation, we studied how the small amount of water absorbed in RTILs responds to the electrode polarization. The results revealed that the enrichment of water near electrodes as the surface charge density increases is likely a universal phenomenon in EDLs formed by RTILs with ions larger than water molecules. The type of ions affects water accumulation, due to the difference of the ion volume/shape and the "subtleties" of water–ion interaction, but it will not change the concave shape of the water accumulation *versus* surface charge curve, although the symmetry of the curve does depend on the type of ions.

We identified several factors that govern the water distribution near electrodes in contact with humid RTILs: (1) interactions between water dipoles and the inhomogeneous electrical field within EDLs, which tend to drive water molecules toward positions where the absolute value of the electrical field reaches local maximum; (2) the association of water molecules with their surrounding ions, which favors stronger accumulation of water molecules at positions where they have better access to the highly charged moieties

of ions; and (3) the availability of free space near the electrode surface where ions could be densely packed. The distribution of water near the electrode is a synergistic effect of these factors. Each of these factors, especially the ion−water association and availability of voids near electrodes, depends directly on the size, shape, intramolecular structure, and charge distribution of the ions. These factors are all affected by the electrode polarization. These dependences are responsible for the ion specificity of water electrosorption and also help explain the asymmetrical dependence of electrosorption on the polarity of the electrode.

The enrichment of water molecules in EDLs formed in humid RTILs can potentially be detrimental to the application of RTILs in electrochemical systems. The water molecules adsorbed on the electrode surface will likely go through electrolysis at voltage lower than the voltage at which neat ionic liquids decompose. Prior studies of RTILs with a moderate to large amount of water (1−50% in volume) showed that electrolysis of water is notable at −0.9 V and strong at −1.4 V.[53,54] Electrolysis at similarly low overvoltage likely will also occur for RTILs with only a very small amount of water (the situation considered in this work), although we must note that the thermodynamics and kinetics of the corresponding electron transfer reactions are big studies of their own which are yet to be performed. Whether the electrolysis of water will effectively remove water molecules from RTILs and how the electrochemical properties of RTILs will be affected by water contents, however, will depend on the specific situation.

If the electrochemical device operates as an open system, electrolysis of water will not necessarily lead to net decrease of the water content in RTILs or near the electrode surface: new water molecules may get into RTILs from the environment and become adsorbed on the electrode. In this case, a continuous leakage current would appear. For larger overvoltages, this process will be controlled by the stationary concentration of water at the electrodes. The exact value of overvoltage for the electrolysis of such impurity water may be different for different ionic liquids[55] because the kinetics of the reaction may be controlled by various factors, such as reorganization energy of the surrounding liquid, matrix elements of transition, diffusion of water, and products of electrolysis—all of these may change with a change of an ionic liquid. On the other hand, the presence of water may affect the electrochemical decomposition of the ionic liquid ions, quite likely reducing the threshold overvoltage for this process, but the effect may be relatively minor. These expectations are qualitative in nature and require systematic experimental validation, but we believe that our study sets the avenues for such tests.

If the electrochemical device is sealed, that is, no water molecules can enter the device, different phenomena may occur. Specifically, electrolysis of the adsorbed water will lead to hydrogen and oxygen evolution at electrode surfaces. Such gas evolution can lead to an increase of the pressure inside the device, and the gas bubble may block the pores of porous electrodes. For supercapacitors, this issue is usually addressed by implementing gas valves, which lets some of the accumulated gases out but does not let water get into the device from the atmosphere. An alternative consequence is that the H^+ and OH^- ions generated during electrolysis start reacting with ionic liquids, changing their chemical composition, which can also lead to degradation of the cell. However, if the generation of the product of electrolysis of any kind does not stall the process of capacitance charging, in a closed system and without abundance of water (such as in hydrophobic ionic liquids), all water molecules will be digested and the system will become stable. Therefore, only a transient leak current will be observed.

We hope that the findings reported here will serve as a stimulus for systematic experimental investigations of the water distribution in double layers by any available *in situ* methods. The small-angle neutron diffraction technique, exploiting isotopic substitution, may provide the needed sensitivity, but it would require very intensive neutron beams to be able to see water deuterons at the background of all other nuclei in RTILs. Two-dimensional infrared spectroscopy may also be tried. Promising for this purpose may be surface enhanced infrared adsorption spectroscopy[61] although it has to be limited to electrodes made of "plasmonic" metals, such as gold or silver. Regardless of what techniques are preferred by experimentalists, we hope that this paper will trigger their curiosity to check the predictions herein. If verified, there will be a definite picture of where and how much water molecules are adsorbed near polarized and nonpolarized electrodes. The insights gained in this work, with more systematic studies of issues such as ion specificity of the electrosorption of water, may then help manage water accumulation near electrodes.

METHODS

The MD system (see Figure 1a) consists of a slab of humid RTILs enclosed between two oppositely charged electrodes. Each electrode is modeled as three layers of graphene sheets with an area of 5.54 × 5.66 nm^2. The graphene layers are arranged in AB stacking with an interlayer spacing of 0.34 nm. Small partial charges are uniformly distributed among carbon atoms of the two graphene sheets in contact with the humid RTIL to create the desired surface charge densities. The distance between the innermost layers of the two electrodes is 8.0 nm,

which should be wide enough to ensure that the RTILs in the central portion of the system are bulk-like (prior simulations have shown that the EDLs formed by similar-sized RTILs have a thickness <3 nm).[44−48] The expectation that RTILs in the central portion of the system are bulk-like is corroborated by the observation that, beyond positions 3.0 nm from the electrode surface, the ionic space charge density is practically zero (*i.e.*, both cations and anions are distributed homogeneously) and the electrical potential profile is flat (see Figure S6). The electronic polarizability of the electrode and the image charge effects are not taken into account in these constant-charge simulations due to the significant computational cost associated with constant-potential simulations. However, since prior studies of the double layers in molten salts and RTILs indicated that key thermodynamic aspects of double layers are captured quite effectively in constant-charge simulations, such an approximate treatment of the electrode is deemed sufficient in the present first study.[56,57]

Two widely studied RTILs, [Bmim][PF_6] and [Bmim][Tf_2N] (Figure 1b−d), were used to assess whether features of water electrosorption observed in our simulations are generic to hydrophobic RTILs with ions larger than water molecules. Both all-atom force fields[58] and coarse-grained force fields[59] have been used for the ionic liquid [Bmim][PF_6]. All-atom force fields were used for the ionic liquid [Bmim][Tf_2N]. The SPC/E model was used for the water molecules; carbon atoms in the electrode were modeled using the force fields in ref 58. In general, the electronic polarizability of water and RTIL molecules should be accounted for by the most accurate description of their interactions and dynamics. However, as prior simulations based on nonpolarizable water/RTIL models have successfully captured key features of the water−RTIL mixture, the force fields adopted here are deemed adequate. In addition, separate simulations, in which all water molecules in the humid RTILs were removed, were performed to evaluate the effects of water contamination on the capacitive properties of the EDLs in RTILs.

Simulations were performed in the NVT ensemble using a customized MD code Gromacs.[60] The electrolyte temperature was maintained at 333 K using the Nosé−Hoover thermostat. The electrostatic interactions were computed using the PME method. An FFT grid spacing of 0.1 nm and cubic interpolation for charge distribution were used to compute the electrostatic interactions in the reciprocal space. A cutoff length of 1.1 nm was used in the calculation of electrostatic interactions in the real space. The nonelectrostatic interactions were computed by direct summation with a cutoff length of 1.1 nm. For each simulation, the MD system was first simulated at 1000 K for 3 ns, and the system temperature was gradually quenched to the target temperature. After that, to reach equilibrium, the simulation was first run for 30 ns and then a 120 ns production run was performed. To ensure the accuracy of the simulation results, each case was repeated three times with different initial configurations.

Since the number of molecules in the humid and neat ionic liquids is different, the pressure in these systems is different. To assess whether pressure affects the electrosorption of water, we reduced the number of ion pairs in the humid [Bmim][PF_6] by 2% (thus reducing the pressure inside the cell). We found that the enhancement of water near electrified electrodes is similar to that observed in the original humid [Bmim][PF_6] (see Figure S7), indicating that pressure plays a minor role in electrosorption in the present systems.

Conflict of Interest: The authors declare no competing financial interest.

Acknowledgment. G.F. acknowledges funding from National Natural Science Foundation of China (51406060) and partial support from Natural Science Foundation of Hubei Province of China (2014CFA089). R.Q. acknowledges the support of the NSF (CBET-1264578). A.A.K. acknowledges useful discussion with Professor Richard Compton at Oxford University. The authors are also thankful to Professor Galina Tsirlina (Moscow State University) for useful, illuminating discussions.

Supporting Information Available: (1) Effects of RTIL humidity and ion loading on the electrosorption of water, (2) electrosorption of water computed using coarse-grained models of [Bmim][PF_6] and all-atom model of [Bmim][Tf_2N], (3) the distribution and orientation of ions and water molecules near electrodes with different surface charge densities, (4) effects of water "contamination" on EDL capacitance, and (5) the distribution of net ionic space charge density and electrical potential profile across the entire cell. This material is available free of charge *via* the Internet at http://pubs.acs.org.

REFERENCES AND NOTES

1. Plechkova, N. V.; Seddon, K. R. Applications of Ionic Liquids in the Chemical Industry. *Chem. Soc. Rev.* **2008**, *37*, 123–150.
2. Krossing, I.; Slattery, J. M.; Daguenet, C.; Dyson, P. J.; Oleinikova, A.; Weingärtner, H. Why Are Ionic Liquids Liquid? A Simple Explanation Based on Lattice and Solvation Energies. *J. Am. Chem. Soc.* **2006**, *128*, 13427–13434.
3. Maruyama, S.; Takeyama, Y.; Taniguchi, H.; Fukumoto, H.; Itoh, M.; Kumigashira, H.; Oshima, M.; Yamamoto, T.; Matsumoto, Y. Molecular Beam Deposition of Nanoscale Ionic Liquids in Ultrahigh Vacuum. *ACS Nano* **2010**, *4*, 5946–5952.
4. Welton, T. Room-Temperature Ionic Liquids. Solvents for Synthesis and Catalysis. *Chem. Rev.* **1999**, *99*, 2071–2083.
5. Maton, C.; De Vos, N.; Stevens, C. V. Ionic Liquid Thermal Stabilities: Decomposition Mechanisms and Analysis Tools. *Chem. Soc. Rev.* **2013**, *42*, 5963–5977.
6. Fedorov, M. V.; Kornyshev, A. A. Ionic Liquids at Electrified Interfaces. *Chem. Rev.* **2014**, *114*, 2978–3036.
7. Péan, C.; Merlet, C.; Rotenberg, B.; Madden, P. A.; Taberna, P.-L.; Daffos, B.; Salanne, M.; Simon, P. On the Dynamics of Charging in Nanoporous Carbon-Based Supercapacitors. *ACS Nano* **2014**, *8*, 1576–1583.
8. Shim, Y.; Kim, H. J. Nanoporous Carbon Supercapacitors in an Ionic Liquid: A Computer Simulation Study. *ACS Nano* **2010**, *4*, 2345–2355.
9. Yusko, E. C.; An, R.; Mayer, M. Electroosmotic Flow Can Generate Ion Current Rectification in Nano- and Micropores. *ACS Nano* **2009**, *4*, 477–487.
10. Ohno, H. *Electrochemical Aspects of Ionic Liquids*; John Wiley & Sons: Hoboken, NJ, 2011.
11. Shen, X.; Sun, B.; Yan, F.; Zhao, J.; Zhang, F.; Wang, S.; Zhu, X.; Lee, S. High-Performance Photoelectrochemical Cells from Ionic Liquid Electrolyte in Methyl-Terminated Silicon Nanowire Arrays. *ACS Nano* **2010**, *4*, 5869–5876.
12. Li, H.; Rutland, M. W.; Atkin, R. Ionic Liquid Lubrication: Influence of Ion Structure, Surface Potential and Sliding Velocity. *Phys. Chem. Chem. Phys.* **2013**, *15*, 14616–14623.
13. Murugesan, S.; Akkineni, A.; Chou, B. P.; Glaz, M. S.; Vanden Bout, D. A.; Stevenson, K. J. Room Temperature Electrodeposition of Molybdenum Sulfide for Catalytic and Photoluminescence Applications. *ACS Nano* **2013**, *7*, 8199–8205.
14. Perkin, S.; Albrecht, T.; Klein, J. Layering and Shear Properties of an Ionic Liquid, 1-Ethyl-3-methylimidazolium Ethylsulfate, Confined to Nano-films between Mica Surfaces. *Phys. Chem. Chem. Phys.* **2010**, *12*, 1243–1247.
15. Simon, P.; Gogotsi, Y. Materials for Electrochemical Capacitors. *Nat. Mater.* **2008**, *7*, 845–854.
16. Armand, M.; Endres, F.; MacFarlane, D. R.; Ohno, H.; Scrosati, B. Ionic-Liquid Materials for the Electrochemical Challenges of the Future. *Nat. Mater.* **2009**, *8*, 621–629.
17. Brandt, A.; Pohlmann, S.; Varzi, A.; Balducci, A.; Passerini, S. Ionic Liquids in Supercapacitors. *MRS Bull.* **2013**, *38*, 554–559.
18. Kim, T. Y.; Lee, H. W.; Stoller, M.; Dreyer, D. R.; Bielawski, C. W.; Ruoff, R. S.; Suh, K. S. High-Performance Supercapacitors Based on Poly(ionic liquid)-Modified Graphene Electrodes. *ACS Nano* **2010**, *5*, 436–442.
19. Lin, R.; Taberna, P.-L.; Fantini, S. B.; Presser, V.; Pérez, C. R.; Malbosc, F. O.; Rupesinghe, N. L.; Teo, K. B. K.; Gogotsi, Y.; Simon, P. Capacitive Energy Storage from −50 to 100 °C

Using an Ionic Liquid Electrolyte. *J. Phys. Chem. Lett.* **2011**, *2*, 2396–2401.
20. Balducci, A.; Dugas, R.; Taberna, P. L.; Simon, P.; Plée, D.; Mastragostino, M.; Passerini, S. High Temperature Carbon–Carbon Supercapacitor Using Ionic Liquid as Electrolyte. *J. Power Sources* **2007**, *165*, 922–927.
21. Choi, B. G.; Yang, M.; Jung, S. C.; Lee, K. G.; Kim, J.-G.; Park, H.; Park, T. J.; Lee, S. B.; Han, Y.-K.; Huh, Y. S. Enhanced Pseudocapacitance of Ionic Liquid/Cobalt Hydroxide Nanohybrids. *ACS Nano* **2013**, *7*, 2453–2460.
22. Wang, H.; Xu, Z.; Kohandehghan, A.; Li, Z.; Cui, K.; Tan, X.; Stephenson, T. J.; King'ondu, C. K.; Holt, C. M. B.; Olsen, B. C.; Tak, J. K.; Harfield, D.; Anyia, A. O.; Mitlin, D. Interconnected Carbon Nanosheets Derived from Hemp for Ultrafast Supercapacitors with High Energy. *ACS Nano* **2013**, *7*, 5131–5141.
23. Wasserscheid, P.; Welton, T. *Ionic Liquids in Synthesis*; Wiley Online Library: New York, 2003.
24. Anthony, J. L.; Maginn, E. J.; Brennecke, J. F. Solution Thermodynamics of Imidazolium-Based Ionic Liquids and Water. *J. Phys. Chem. B* **2001**, *105*, 10942–10949.
25. Rivera-Rubero, S.; Baldelli, S. Influence of Water on the Surface of Hydrophilic and Hydrophobic Room-Temperature Ionic Liquids. *J. Am. Chem. Soc.* **2004**, *126*, 11788–11789.
26. Lynden-Bell, R. M.; Kohanoff, J.; Del Popolo, M. G. Simulation of Interfaces between Room Temperature Ionic Liquids and Other Liquids. *Faraday Discuss.* **2005**, *129*, 57–67.
27. Jiang, W.; Wang, Y.; Voth, G. A. Molecular Dynamics Simulation of Nanostructural Organization in Ionic Liquid/Water Mixtures. *J. Phys. Chem. B* **2007**, *111*, 4812–4818.
28. Wang, Y.; Kakiuchi, T.; Yasui, Y.; Mirkin, M. V. Kinetics of Ion Transfer at the Ionic Liquid/Water Nanointerface. *J. Am. Chem. Soc.* **2010**, *132*, 16945–16952.
29. Hayes, R.; Imberti, S.; Warr, G. G.; Atkin, R. How Water Dissolves in Protic Ionic Liquids. *Angew. Chem.* **2012**, *124*, 7586–7589.
30. Terranova, Z. L.; Corcelli, S. A. Molecular Dynamics Investigation of the Vibrational Spectroscopy of Isolated Water in an Ionic Liquid. *J. Phys. Chem. B* **2014**, *118*, 8264–8272.
31. Khan, I.; Taha, M.; Ribeiro-Claro, P.; Pinho, S. P.; Coutinho, J. A. P. Effect of the Cation on the Interactions between Alkyl Methyl Imidazolium Chloride Ionic Liquids and Water. *J. Phys. Chem. B* **2014**, *118*, 10503–10514.
32. Sieffert, N.; Wipff, G. The [BMI][Tf_2N] Ionic Liquid/Water Binary System: A Molecular Dynamics Study of Phase Separation and of the Liquid–Liquid Interface. *J. Phys. Chem. B* **2006**, *110*, 13076–13085.
33. Maerzke, K. A.; Goff, G. S.; Runde, W. H.; Schneider, W. F.; Maginn, E. J. Structure and Dynamics of Uranyl(VI) and Plutonyl(VI) Cations in Ionic Liquid/Water Mixtures *via* Molecular Dynamics Simulations. *J. Phys. Chem. B* **2013**, *117*, 10852–10868.
34. Cammarata, L.; Kazarian, S. G.; Salter, P. A.; Welton, T. Molecular States of Water in Room Temperature Ionic Liquids. *Phys. Chem. Chem. Phys.* **2001**, *3*, 5192–5200.
35. Moreno, M.; Castiglione, F.; Mele, A.; Pasqui, C.; Raos, G. Interaction of Water with the Model Ionic Liquid [Bmim][BF_4]: Molecular Dynamics Simulations and Comparison with NMR Data. *J. Phys. Chem. B* **2008**, *112*, 7826–7836.
36. D'Angelo, P.; Zitolo, A.; Aquilanti, G.; Migliorati, V. Using a Combined Theoretical and Experimental Approach To Understand the Structure and Dynamics of Imidazolium-Based Ionic Liquids/Water Mixtures. 2. EXAFS Spectroscopy. *J. Phys. Chem. B* **2013**, *117*, 12516–12524.
37. Porter, A. R.; Liem, S. Y.; Popelier, P. L. A. Room Temperature Ionic Liquids Containing Low Water Concentrations—A Molecular Dynamics Study. *Phys. Chem. Chem. Phys.* **2008**, *10*, 4240–4248.
38. Menjoge, A.; Dixon, J.; Brennecke, J. F.; Maginn, E. J.; Vasenkov, S. Influence of Water on Diffusion in Imidazolium-Based Ionic Liquids: A Pulsed Field Gradient Nmr Study. *J. Phys. Chem. B* **2009**, *113*, 6353–6359.
39. Kelkar, M. S.; Maginn, E. J. Effect of Temperature and Water Content on the Shear Viscosity of the Ionic Liquid 1-Ethyl-3-methylimidazolium Bis(trifluoromethanesulfonyl)imide As Studied by Atomistic Simulations. *J. Phys. Chem. B* **2007**, *111*, 4867–4876.
40. Bhargava, B. L.; Yasaka, Y.; Klein, M. L. Computational Studies of Room Temperature Ionic Liquid–Water Mixtures. *Chem. Commun.* **2011**, *47*, 6228–6241.
41. Feng, S.; Voth, G. A. Molecular Dynamics Simulations of Imidazolium-Based Ionic Liquid/Water Mixtures: Alkyl Side Chain Length and Anion Effects. *Fluid Phase Equilib.* **2010**, *294*, 148–156.
42. Cuadrado-Prado, S.; Domínguez-Pérez, M.; Rilo, E.; García-Garabal, S.; Segade, L.; Franjo, C.; Cabeza, O. Experimental Measurement of the Hygroscopic Grade on Eight Imidazolium Based Ionic Liquids. *Fluid Phase Equilib.* **2009**, *278*, 36–40.
43. Leenaerts, O.; Partoens, B.; Peeters, F. M. Water on Graphene: Hydrophobicity and Dipole Moment Using Density Functional Theory. *Phys. Rev. B* **2009**, *79*, 235440.
44. Vatamanu, J.; Borodin, O.; Smith, G. D. Molecular Insights into the Potential and Temperature Dependences of the Differential Capacitance of a Room-Temperature Ionic Liquid at Graphite Electrodes. *J. Am. Chem. Soc.* **2010**, *132*, 14825–14833.
45. Israelachvili, J. N. *Intermolecular and Surface Forces*; Academic Press: New York, 1992.
46. Vatamanu, J.; Borodin, O.; Smith, G. D. Molecular Simulations of the Electric Double Layer Structure, Differential Capacitance, and Charging Kinetics for *N*-Methyl-*N*-propylpyrrolidinium Bis(fluorosulfonyl)imide at Graphite Electrodes. *J. Phys. Chem. B* **2011**, *115*, 3073–3084.
47. Kornyshev, A. A. Double-Layer in Ionic Liquids: Paradigm Change? *J. Phys. Chem. B* **2007**, *111*, 5545–5557.
48. Vatamanu, J.; Borodin, O.; Bedrov, D.; Smith, G. D. Molecular Dynamics Simulation Study of the Interfacial Structure and Differential Capacitance of Alkylimidazolium Bis(trifluoromethanesulfonyl)imide [$C_n$mim][TFSI] Ionic Liquids at Graphite Electrodes. *J. Phys. Chem. C* **2012**, *116*, 7940–7951.
49. Lanning, O. J.; Madden, P. A. Screening at a Charged Surface by a Molten Salt. *J. Phys. Chem. B* **2004**, *108*, 11069–11072.
50. Lynden-Bell, R. M.; Frolov, A. I.; Fedorov, M. V. Electrode Screening by Ionic Liquids. *Phys. Chem. Chem. Phys.* **2012**, *14*, 2693–2701.
51. The dominance of energetic effects over the entropic effect is also supported by the observation that, near moderately charged electrodes, water molecules near the electrode align very well with the electrical field.
52. Chang, T. M.; Peterson, K. A.; Dang, L. X. Molecular Dynamics Simulations of Liquid, Interface, and Ionic Solvation of Polarizable Carbon Tetrachloride. *J. Chem. Phys.* **1995**, *103*, 7502–7513.
53. de Souza, R. F.; Padilha, J. C.; Gonçalves, R. S.; Rault-Berthelot, J. Dialkylimidazolium Ionic Liquids as Electrolytes for Hydrogen Production from Water Electrolysis. *Electrochem. Commun.* **2006**, *8*, 211–216.
54. de Souza, R. F.; Padilha, J. C.; Gonçalves, R. S.; de Souza, M. O.; Rault-Berthelot, J. Electrochemical Hydrogen Production from Water Electrolysis Using Ionic Liquid as Electrolytes: Towards the Best Device. *J. Power Sources* **2007**, *164*, 792–798.
55. Lu, X.; Burrell, G.; Separovic, F.; Zhao, C. Electrochemistry of Room Temperature Protic Ionic Liquids: A Critical Assessment for Use as Electrolytes in Electrochemical Applications. *J. Chem. Phys. B* **2012**, *116*, 9160–9170.
56. Reed, S. K.; Lanning, O. J.; Madden, P. A. Electrochemical Interface between an Ionic Liquid and a Model Metallic Electrode. *J. Chem. Phys.* **2007**, *126*, 084704.
57. Merlet, C. l.; Salanne, M.; Rotenberg, B.; Madden, P. A. Imidazolium Ionic Liquid Interfaces with Vapor and Graphite: Interfacial Tension and Capacitance from Coarse-Grained Molecular Simulations. *J. Phys. Chem. C* **2011**, *115*, 16613–16618.

58. Canongia Lopes, J. N.; Pádua, A. A. H. Molecular Force Field for Ionic Liquids Composed of Triflate or Bistriflylimide Anions. *J. Phys. Chem. B* **2004**, *108*, 16893–16898.
59. Merlet, C.; Rotenberg, B.; Madden, P. A.; Taberna, P.-L.; Simon, P.; Gogotsi, Y.; Salanne, M. On the Molecular Origin of Supercapacitance in Nanoporous Carbon Electrodes. *Nat. Mater.* **2012**, *11*, 306–310.
60. Lindahl, E.; Hess, B.; van der Spoel, D. Gromacs 3.0: A Package for Molecular Simulation and Trajectory Analysis. *J. Mol. Model.* **2001**, *7*, 306–317.
61. Motobayashi, K.; Minami, K.; Nishi, N.; Sakka, T.; Osawa, M. Hysteresis of Potential-Dependent Changes in Ion Density and Structure of an Ionic Liquid on a Gold Electrode: *In Situ* Observation by Surface-Enhanced Infrared Absorption Spectroscopy. *J. Phys. Chem. Lett.* **2013**, *4*, 3110–3114.